Thermal stability, sensitivity, and noise characteristics of MgO-based magnetic tunnel junctions (invited)

Dipanjan Mazumdar[a)]
Physics Department, Brown University, Providence, Rhode Island 02912

Xiaoyong Liu and B. D. Schrag
Physics Department, Brown University, Providence, Rhode Island 02912 and MicroMagnetics Inc., Fall River, Massachusetts 02720

Weifeng Shen
Physics Department, Brown University, Providence, Rhode Island 02912

Matthew Carter
MicroMagnetic Inc., Fall River, Massachusetts 02912

Gang Xiao
Physics Department, Brown University, Providence, Rhode Island 02912

(Presented on 10 January 2007; received 31 October 2006; accepted 7 December 2006; published online 27 April 2007)

Thermal stability, sensitivity, and noise of micron-scale magnetic tunnel junctions based on MgO tunnel barriers have been studied for both the memory and sensing configurations. Junctions show solid high-temperature performance with substantial magnetoresistance observed even at 500 °C. At temperatures above 375 °C, the junctions begin to experience irreversible degradation due to interlayer diffusion. The thermal stability of these devices depends strongly on the exchange bias of the device and hence on the properties of the antiferromagnetic layer. Sensitivities as high as 3.3%/Oe have been obtained at room temperature for junctions configured as low-field sensors. Sensitivity values are constant up to temperatures of 300 °C, above which performance decays due to a loss of exchange bias and overall magnetoresistance. Noise spectra are $1/f$ at frequencies up to 51 kHz, and sensors have a resultant field noise better than 1 $nT/Hz^{0.5}$ at 100 kHz. A comparison is made with devices fabricated with alumina tunnel barriers. © *2007 American Institute of Physics*. [DOI: 10.1063/1.2710953]

Spintronics research got a major boost with the successful fabrication of high magnetoresistance (MR) magnetic tunnel juctions (MTJs) with MgO as the insulating barrier layer. Highly ordered (100) MgO growth is the key for such a realization.[1–3] Since the initial reports in 2004 by IBM (Ref. 4) and AIST,[5] some other groups have successfully reported samples with similarly high MR values.[6–8] The bulk of MTJ research focuses on the application to magnetic random access memory (MRAM), for which high MR values lead directly to high on/off ratios and hence enhanced bit performance. In this paper we will report on some of the issues and practical applications of MgO-based devices, with a focus on low-field sensor applications. For instance, the high MR ratio has definitely opened the door to a wider range of potential applications beyond what can be achieved with alumina sensors. We shall discuss in some detail the thermal performance of junctions at temperatures as high as 500 °C, in both the memory and sensor configurations. From the standpoint of a magnetic sensor, sensitivity and noise are the two most important yardsticks. In the sensor configuration, sensitivity in excess of 1.5%/Oe has been consistently obtained in small junctions, a value which is almost an order of magnitude higher than comparable alumina-based sensors.

We extend on traditional sensitivity measurements by measuring device sensitivity as a function of both sensing and longitudinal applied fields. The resulting data are plotted in a two-dimensional "sensitivity map," which offers information about sensor anisotropy and related parameters. These sensitivity maps are similar to the more traditional Stoner-Wohlfarth asteroid curves, which have been used to understand the switching characteristics of memory-configuration devices for MRAM applications.[9]

Noise measurements on micron-size sensors yield a field noise value of ~950 $pT/Hz^{0.5}$ at 100 kHz, a value which is lower than what was previously reported for alumina-based sensors. However, the raw voltage noise in MgO-based sensors is higher than that in alumina-based devices for all junctions which we have measured. The low-frequency voltage noise is $1/f$ in nature, as expected from many previous results.[10–12] Our data also indicate that the noise source is predominantly magnetic in origin and that this noise is caused by thermal magnetization fluctuations of the free layer.

The MTJ layer structure used for this work was Ta(300)/$Co_{50}Fe_{50}$(30)/IrMn(150)/$Co_{50}Fe_{50}$(20)/Ru(8)/$Co_{40}Fe_{40}B_{20}$(30)/MgO(12)/$Co_{40}Fe_{40}B_{20}$(30)/Ta(100)/Ru(150) (thicknesses in angstroms). This multilayer structure was grown by magnetron sputtering onto thermally oxidized 2 in.

[a)]Electronic mail: mazumdar@physics.brown.edu

Si wafers. An *in situ* field of ~100 Oe was applied during deposition to induce a uniaxial anisotropy in the free layer as well as an exchange bias. Junctions were patterned to small sizes using standard lithographic techniques. After device fabrication, junctions were annealed at 380 °C in a high vacuum (5×10^{-7} Torr) and high applied field (2.5 kOe) for 1 h in order to improve the exchange bias as well as allow crystallization of the amorphous CoFeB electrode layers, which leads to a huge enhancement in MR ratio.[6,7] More details about our deposition and processing steps are given in Ref. 8 All junctions used in this study were elliptical in shape, with lateral dimensions ranging from 2 to 6 μm. Transport measurements were done using a dc four-point method.

The applied field direction during the annealing process determines the pinning direction of the pinned layer via exchange bias. MTJ devices in the sensor (memory) configuration are annealed such that the magnetization of the pinned layer is perpendicular (parallel) to the easy axis of the free layer. Additionally, a permanent magnetic (PM) film is patterned adjacent to the sensor area for MTJs in the sensor configuration. This added layer provides a longitudinal bias field, which reduces hysteresis and creates a more linear sensor response.

High-temperature performance was examined in air. Wafers were mounted on a heated stage with low thermal mass inside our standard magnetotransport measurement apparatus. A thermocouple and proportional-integral-derivative (PID) controller were used to measure and control the wafer temperature during these studies.

In order to maintain a higher-temperature stability, an antiferrimagnetically coupled synthetic CoFe(20)/Ru/CoFeB(30) trilayer structure has been used in place of the traditional pinned electrode layer. This structure provides two benefits. It increases the physical separation between the antiferromagnetic (AFM) layer and the insulating MgO barrier layer, which reduces the rate of diffusion of Mn^{+} ions, which is known to degrade the barrier quality at high temperatures.[13,14] This structure also ensures a stronger and more thermally stable exchange bias than a simple ferromagnetic (FM)/AFM bilayer. IrMn pinning layers are widely used due to its improved thermal stability.[15]

Amorphous CoFeB has become the most popular choice of material for the FM electrodes in MTJ devices with MgO as the tunnel barrier. This material has high spin polarization and good growth properties. This amorphous material also serves as a diffusion barrier and has been reported to yield larger MR ratios and better thermal stability than polycrystalline electrodes, such as CoFe, after high temperature annealing.[16] High resolution transmission electron microscopy (TEM) images as well as theoretical predictions have suggested that large MR ratios depend critically on the realization of a smooth (100) crystal orientation at both the CoFeB–MgO interfaces. The primary goal of the annealing process is to allow the CoFeB layer to crystallize into the (100) structure.[6,7]

Figure 1 shows the room-temperature (RT) magnetoresistance transfer curve of a memory-type junction with 260% total magnetoresistance. Junctions used in this work all have

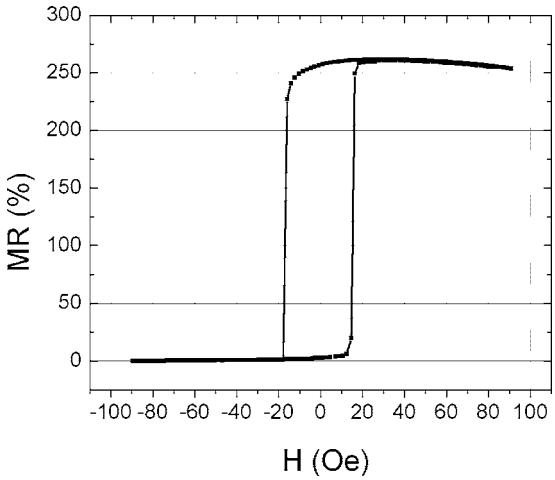

FIG. 1. Room-temperature transfer curve of a junction in the memory configuration. The total magnetoresistance is 260%.

MR ratios of over 200% at room temperature. Figure 2 gives the variation of MR ratio for a typical junction as a function of temperature. The temperature was ramped at 5 °C/min and allowed to stabilize before each measurement. At temperatures less than ~250 °C, the MR degrades slowly, without any significant changes in the sensor transfer curves [(a)–(c)]. The MR drops to half its RT value at 300 °C. Beyond 300 °C both exchange bias and MR start to degrade at a much faster rate. By a temperature of 450 °C, exchange bias is completely lost [(e) and (f)] and the MR ratio drops below 10% at 475 °C. The loss in exchange bias at this elevated temperature was permanent, and very low MR was observed when the sample was cooled down to room temperature. The loss in exchange bias indicates that the junction was heated above the blocking temperature, which is estimated to be between 350–450 °C from the transfer curves. This was confirmed by annealing the junction again at 380 °C in vacuum for 1 h. The exchange bias was recovered (reversible effect), but the magnetoresistance was only partially restored (MR ~ 30%), as seen in Fig. 3. The permanent loss in MR suggests irreversible degradation due to diffusion at temperatures above 400 °C. The postannealing MR curve suggests some rotation in either the pinned layer or the anisotropy direction, which may explain the transfer curve, which is less square than that of a normal memory-type MTJ. The exact reason for this is not clear, but it is likely a result of the extended thermal stressing experienced by this device during the annealing process.

A closer look at the thermal dependence of the resistance in the parallel (P) and antiparallel (AP) states shows that the drop in magnetoresistance is primarily due to a drop in the AP-state resistance (Fig. 4). The P-state resistance (indicated by the *RA* product shown in Fig. 4) varies very little below 400 °C. Above this temperature, both the P and AP resistance values begin to increase rapidly. This temperature dependence is in contrast with earlier studies of alumina-based MTJs, where both the P and AP resistances were observed to decrease steadily over the entire range of temperatures.[17] The stability of the parallel-state resistance has also been observed in voltage bias dependence of MgO junctions from our experiments and elsewhere, where the parallel state re-

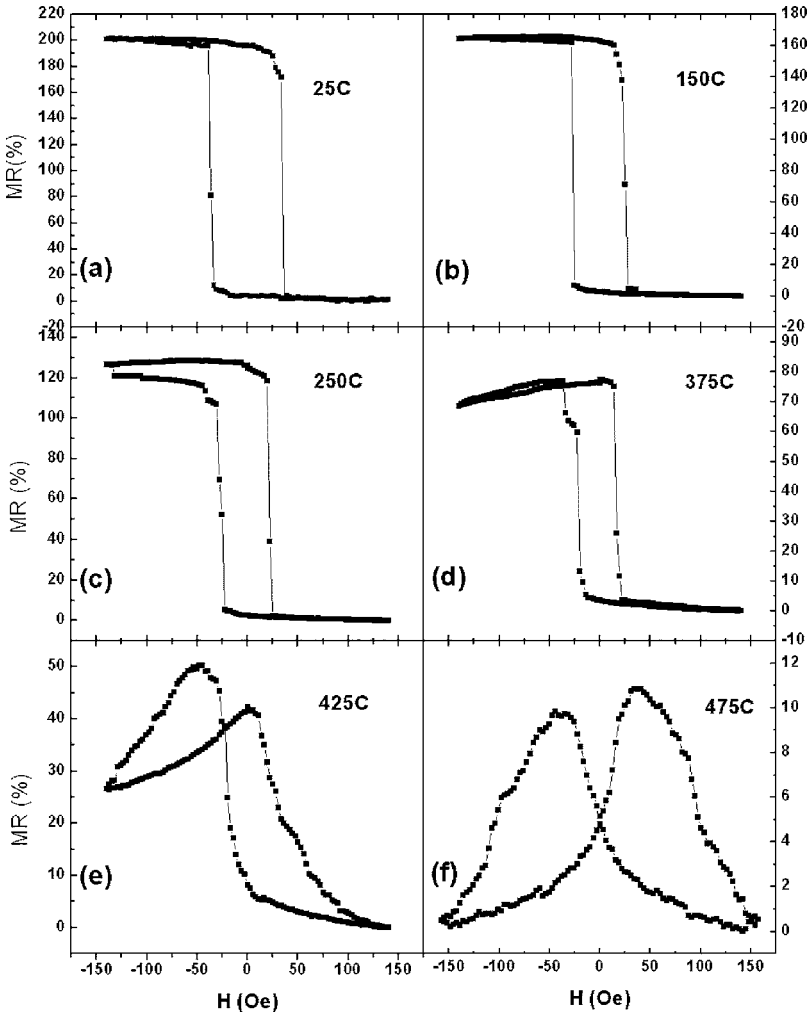

FIG. 2. MR curves as a function of temperature: (a) 25 °C, (b) 150 °C, (c) 250 °C, (d) 375 °C, (e) 425 °C, and (f) 475 °C.

sistance remains constant for a reasonably large bias voltage and the bias dependence of MR is again due to the drop in AP resistance. No thorough theoretical treatment of either the temperature or bias dependence of conductance of a crystalline barrier has been published. A more in-depth explanation of the observed thermal dependence was published previously.[18] This work explains the observed behavior using an empirical $T^{-\alpha}$ $(1<\alpha<2)$ dependence of the spin polarization of the FM electrode and by assuming that conductance can be modeled as the sum of a spin-dependent and a spin-independent conductance.

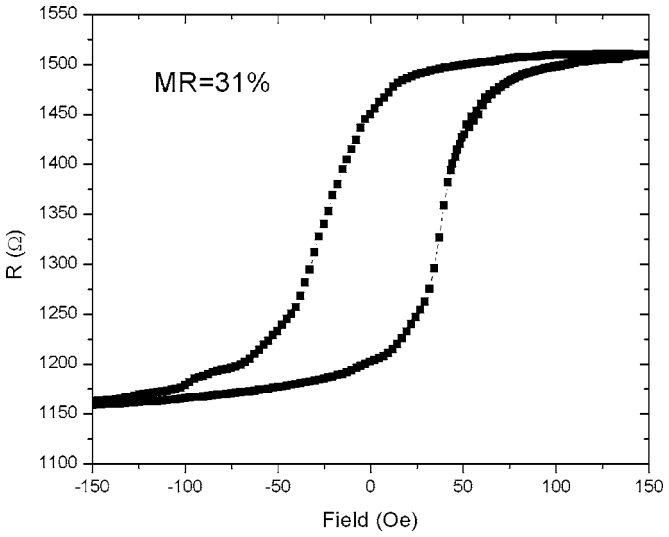

FIG. 3. Magnetoresistance transfer curve of the same sample after reannealing at 380 °C for 1 h.

The temperature behavior of MTJs in the sensor configuration is similar to what was observed in the memory configuration. The drop in MR is primarily due to a decrease in the AP-state resistance, as shown in Fig. 5(a). At temperatures from 25 upto ~300 °C, both dR/dH and R decrease at a uniform rate, which results in a sensitivity which stays roughly constant at 1%/Oe [Fig. 5(b)]. A similar trend was also observed in the other devices which were measured.

For sensor-type tunnel junctions, the field sensitivity is a more important benchmark than the total magnetoresistance. The voltage sensitivity of a MTJ field sensor is in general proportional to the slope of the MR transfer curve (dR/dH) divided by the junction resistance R. In many cases, sensitivity values can be extracted directly from sensor transfer curves. However, if transfer curves exhibit hysteresis, the useful sensitivity can often be less than is expected from the measured slope of the transfer curve. In addition, each branch of a given transfer curve can result in a different sensitivity value. This problem can be circumvented by a direct measurement of the sensitivity as follows. The sensor is subjected to external fields in the two in-plane directions.

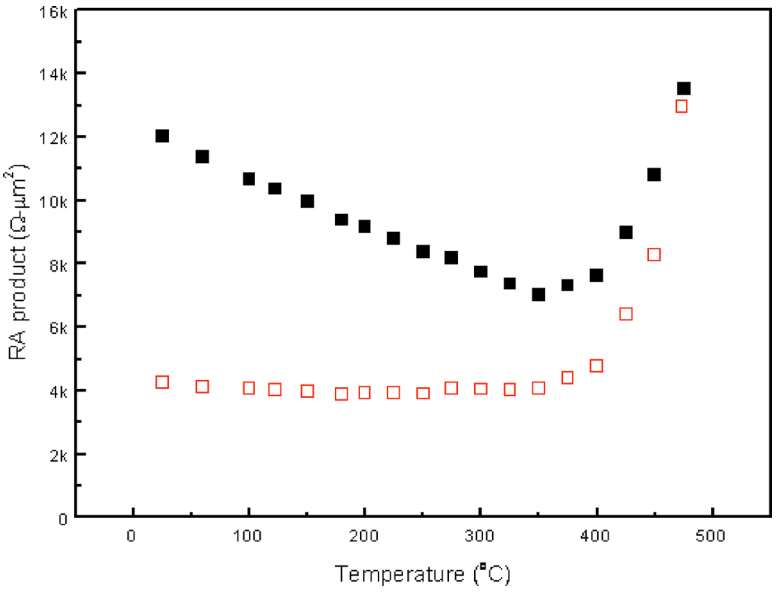

FIG. 4. (Color online) Temperature dependence of the resistance-area product for a typical memory-configuration junction in the parallel (red) and antiparallel (black) states.

In addition, a small (~1–3 Oe), slow ac field in the sensing direction is applied to the sensor. The ac voltage response resulting from this excitation field, as well as the average sensor resistance, is then monitored as the two dc field components are changed. In this way, we obtain traditional hysteresis loops as well as the "true" small-field sensitivity of the sensor for any combination of applied fields. This method is not only more accurate than a simple measurement of the slope but also more versatile. The resulting sensitivity data can be plotted in much the same way as a traditional Stoner-Wohlfarth (SW) "asteroid" curve. This so-called sensitivity map yields information about the device under test, including its anisotropy, easy- and hard-axis coupling fields, and the optimal field biasing conditions for maximal sensitivity. It thus can act as a tool to help optimize sensor design.

The RT sensitivity value for all our MgO sensors is greater than 1%/Oe, and values as high as 3.3%/Oe have been observed [Fig. 5(c)]. A typical nonzero field minor hysteresis loop is shown in Fig. 6(a). The best-fit line to these data corresponds to a sensor sensitivity of 1.8%/Oe. The

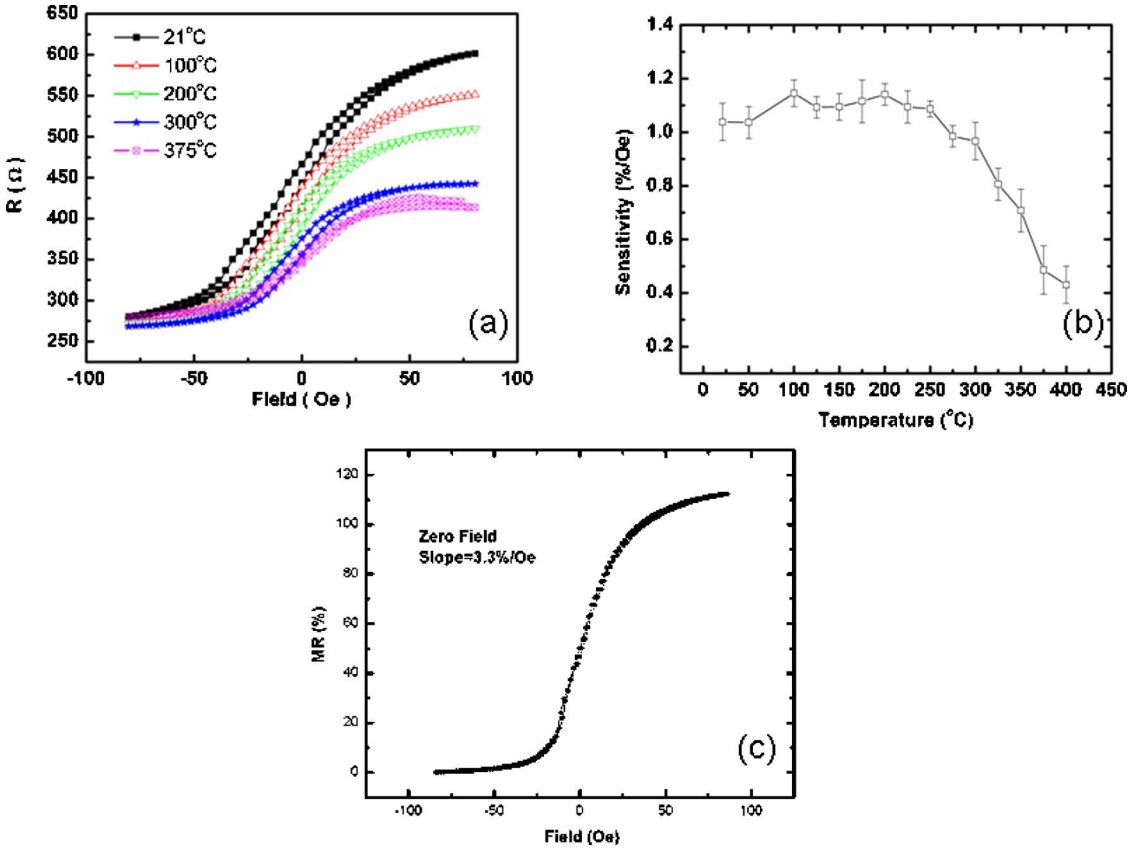

FIG. 5. (Color online) (a) Temperature dependent MR transfer curves of a junction in the sensor configuration. (b) Variation of device sensitivity, calculated from the transfer curve, as a function of temperature. (c) Transfer curve of a MgO sensor showing 3.3%/Oe zero field sensitivity at RT.

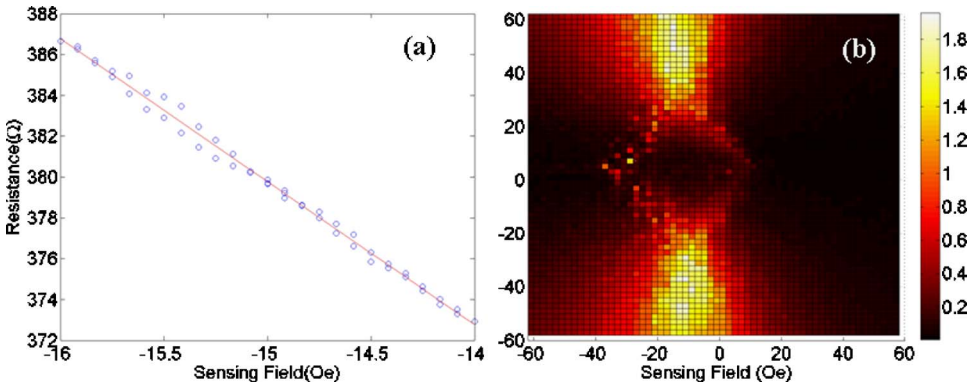

FIG. 6. (Color online) (a) Nonzero field minor hysteresis loop (blue) of a sensor with sensitivity of 1.8%/Oe. The sensitivity value is extracted from a linear fit to the data (red). (b) The sensitivity map of the same sensor. At each field point (H_x, H_y), the sensitivity is calculated from the slope of the minor loop.

average hysteresis over this field range is less than 0.2 Oe. Figure 6(b) shows a sensitivity map as a function of applied fields in the easy (H_x) and hard (H_y) directions. The map shows the average of both the increasing- and decreasing-field hysteresis loops. From the map, a faint outline corresponding to the SW asteroid curve is also seen at field ranges between ±20 Oe. It is readily apparent that the regions of highest sensitivity are located just outside of the asteroid, as expected from the SW model for a device with pinned layer orientation parallel to the induced anisotropy. Hence, the realization of a sensor operating at high sensitivity requires a high hard-axis bias field (at least 35 G in this case). Our previous studies have shown that for single domain MTJ sensors, maximal sensitivity occurs when the longitudinal (i.e., hard axis) bias field is slightly larger than the effective anisotropy field of the free layer. In many cases, the multidomain nature of micron-size samples and the associated Barkhausen jumps are not negligible, and a slightly stronger biasing field is needed to further linearize the sensor response. Additionally, it is clear from the map that there exists a finite offset in the sensing (i.e., easy axis) direction, which is likely due to interlayer coupling between the pinned and free electrodes. Therefore, obtaining optimum sensor response would also require a small bias field in the sensing direction. This bias field is, however, clearly not as critical as the one in the hard-axis direction.

Low-frequency noise measurements were carried out using cross-correlation techniques. The whole setup was put in a shielded environment to eliminate spurious electromagnetic noise sources. In order to minimize the system noise, the circuit is dc powered with a battery and the bias voltage is adjusted using two metal-film potentiometers. A custom-made amplification board comprised of two two-stage low-noise amplification stages is used to amplify the two signal channels, which are needed to calculate the cross spectrum. The dc voltage on each channel is blocked with a large capacitor. The amplified signals are fed into an HP35670A spectrum analyzer, which calculates the power spectral density (PSD) at frequencies from 1 Hz to 51.2 kHz. The system was regularly calibrated with ordinary metal-film resistors to ensure that any background noise was well below the measured junction noise. For all measurements, the junctions were biased with 200 mV, which is a typical operating voltage for our MTJ sensors.

Figure 7(a) compares the normalized voltage noise spectra of a MgO-based sensor with that of an alumina-based sensor at RT. Both spectra are strongly $1/f$ in character throughout the measurement range. The noise of all sensors was also seen to scale with the square of the bias voltage according to Hooge's relation. Although MgO-based sensors have a much higher sensitivity than AlO_x-based devices because of the larger MR ratio, our studies have shown that for sensors with similar sizes, alumina junctions have lower normalized voltage noise. For instance, the average normalized voltage noise for a MgO sensor is 2×10^{-6} $Hz^{-0.5}$ at 1 kHz while that for alumina is 4×10^{-7} $Hz^{-0.5}$. The field noise,

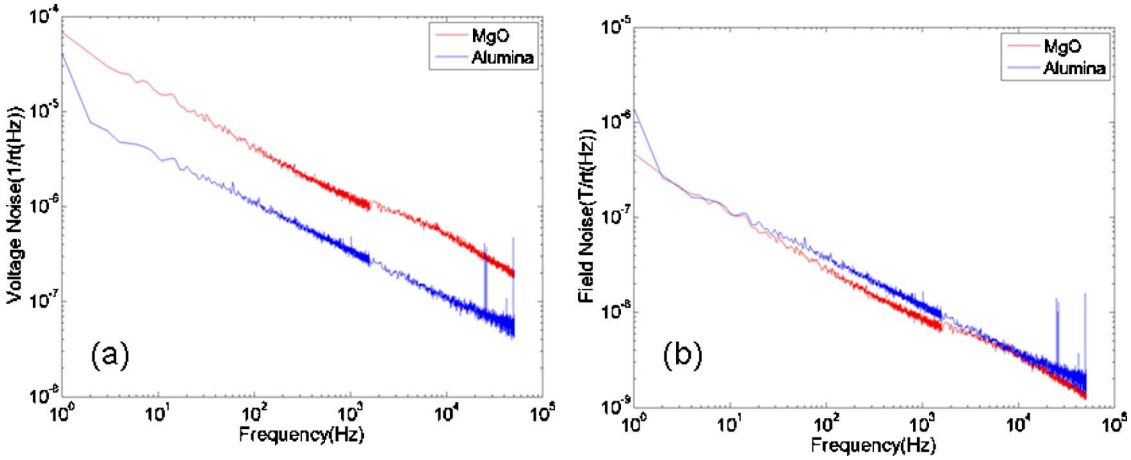

FIG. 7. (Color online) (a) Normalized voltage noise of MgO-based (red) and alumina-based (blue) sensors. Both sensors are field biased to the point of maximum sensitivity. (b) Plots of the corresponding field noise spectra.

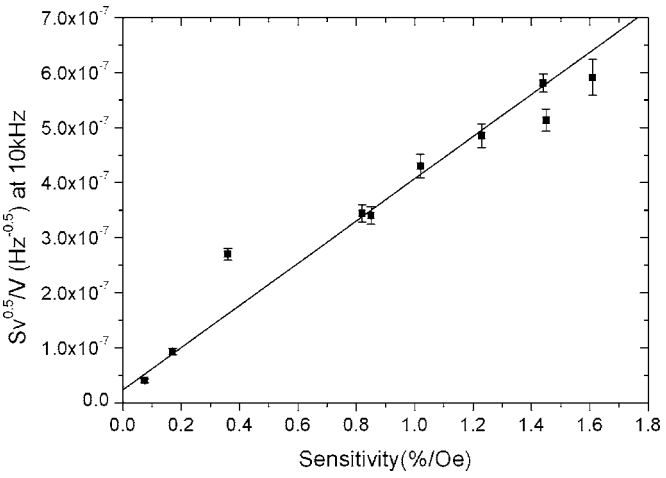

FIG. 8. Normalized voltage noise vs sensitivity for the MgO-based sensor shown in Fig. 7. The linear relationship suggests a magnetic origin for the dominant noise source. The electric and the magnetic component of the noise can be extracted from the intercept and the slope of the linear fit.

defined as the normalized voltage noise divided by the field sensitivity, is shown in Fig. 7(b). From this figure it can be seen that MgO-based sensors have a field noise slightly better than that measured for alumina-based sensors. At 10 kHz, the values for MgO and alumina-based junctions are 3.0 and 3.5 $nT/Hz^{0.5}$, respectively. Assuming perfect $1/f$ dependence, this translates into a field noise of ~ 950 $pT/Hz^{0.5}$ at 100 kHz for MgO-based sensors.

We have also measured magnetic field dependence of noise in MgO-based sensors. Figure 8 plots the measured sensitivity versus the measured noise for the same sensor. It is noted that a roughly linear relationship exists; the solid line plotted in Fig. 8 is a best-fit line to the data. According to earlier work on MTJ devices,[19] the two dominant $1/f$ noise sources which we expect to encounter are electrical noise, which is independent of sensor sensitivity, and magnetic noise, which is caused by magnetization fluctuations of the free layer and which should scale with the sensor sensitivity. The equation of the best-fit line in Fig. 8 allows us to extract each of these noise sources independently. We find that for this sensor, the normalized electrical noise is equal to a sensitivity-independent $(23.3 \pm 3.3) \times 10^{-9}$ $Hz^{-0.5}$, while the magnetic noise is proportional to the device sensitivity with a proportionality constant of (3.8 ± 0.1) $nT/Hz^{0.5}$. This proportionality constant sets a limit on the ultimate field resolution of the sensor; even if the sensitivity is increased, the increased noise will cancel out any gains in sensor performance. Therefore, reducing the slope of this line is the primary challenge involved in improving sensor performance.

We have shown that the thermal behavior of magnetoresistance in a MgO-based MTJ can be explained by considering the temperature dependence of the spin polarization of the free layer. A decline in junction magnetoresistance at high temperatures results from a loss of exchange bias and interlayer diffusion. It is suspected that the observed permanent degradation in sensor performance results primarily from interlayer diffusion, as restoration of exchange bias does not fully restore the MR ratio. The thermal stablity of the AFM layer is crucial for high-temperature operation of MTJ sensors. We have confirmed that the sensitivity of MTJ sensors with IrMn pinning layers and synthetic pinned electrodes remains relatively constant up to 300 °C. The primary noise source in our sensors is $1/f$, with a magnetic origin. As a result, high sensitivity devices also exhibit the largest noise. At high voltage bias (>200 mV), $1/f$ noise totally dominates the noise spectra at frequencies below 100 kHz. Finally, the measured field noise of micron-size MgO-based sensors at 100 kHz is ~ 950 $pT/Hz^{0.5}$. This value further substantiates the potential of MgO-based tunnel junction devices for application as low-field magnetic sensors. Our data also show that the magnetic field noise is typically much higher than the electric noise.

This work was supported at Brown University by the National Science Foundation Grant No. DMR-0605966 and at Micro Magnetics, Inc. by the Advanced Technology Program of the National Institute of Standards and Technology.

[1] W. H. Butler, X.-G. Zhang, T. C. Schulthess, and J. M. MacLaren, Phys. Rev. B **63**, 054416 (2001).
[2] W. H. Butler, X.-G. Zhang, S. Vutukuri, M. Chshiev, and T. C. Schulthess, IEEE Trans. Magn. **41**, 2645 (2005).
[3] J. Mathon and A. Umerski, Phys. Rev. B **63**, 220403R (2001).
[4] S. S. P. Parkin, C. Kaiser, A. Panchula, P. M. Rice, B. Hughes, M. Samant, and S.-H. Yang, Nat. Mater. **3**, 862 (2004).
[5] S. Yuasa, T. Nagahama, A. Fukushima, Y. Suzuki, and K. J. Ando, Nat. Mater. **3**, 868 (2004).
[6] D. D. Djayaprawira, K. Tsunekawa, M. Nagai, H. Maehara, S. Yamagata, and N. Watanabe, Appl. Phys. Lett. **86**, 092502 (2005).
[7] S. Ikeda, J. Hayakawa, Y. M. Lee, R. Sasaki, T. Meguro, F. Matsukura, and H. Ohno, Jpn. J. Appl. Phys., Part 2 **44**, L1442 (2005).
[8] W. Shen, D. Mazumdar, X. Zou, X. Liu, B. D. Schrag, and G. Xiao, Appl. Phys. Lett. **88**, 182508 (2006).
[9] A. Anguelouch, B. D. Schrag, G. Xiao, Y. Lu, P. L. Trouilloud, R. A. Wanner, W. J. Gallagher, and S. S. P. Parkin, Appl. Phys. Lett. **76**, 622 (2000).
[10] A. Gokce, E. R. Nowak, S. H. Yang, and S. S. P. Parkin, J. Appl. Phys. **99**, 08A906 (2006).
[11] A. F. M. Nor, T. Kato, S. J. Ahn, T. Daibou, K. Ono, M. Oogane, Y. Ando, and T. Miyazaki, J. Appl. Phys. **99**, 08T306 (2006).
[12] R. Ferreira, P. Wisniowski, P. P. Freitas, J. Langer, B. Ocker, and W. Maass, J. Appl. Phys. **99**, 08K706 (2006).
[13] R. C. Sousa, J. J. Sun, V. Soares, P. P. Freitas, A. Kling, M. F. da Silva, and J. C. Soares, J. Appl. Phys. **85**, 5258 (1999).
[14] S. Cardoso, R. Ferreira, P. P. Freitas, P. Wei, and J. C. Soares, Appl. Phys. Lett. **76**, 3792 (2000).
[15] J. P. King, J. N. Chapman, M. F. Gillies, and J. C. S. Kools, J. Phys. D **34**, 528 (2001).
[16] T. Dimopoulos, G. Gieres, J. Wecker, N. Wiese, and M. D. Sacher, J. Appl. Phys. **96**, 6382 (2004).
[17] C. H. Shang, J. Nowak, R. Jansen, and J. S. Moodera, Phys. Rev. B **58**, R2917 (1998).
[18] X. Liu, D. Mazumdar, W. Shen, B. D. Schrag, and G. Xiao, Appl. Phys. Lett. **89**, 203504 (2006).
[19] C. Ren, X. Liu, B. D. Schrag, and G. Xiao, Phys. Rev. B **69**, 104405 (2004).